Mon. Not. R. astr. Soc. (1986) **222,** 307–322

Expanding chromospheres of late G and K supergiants

Sushma V. Mallik *Indian Institute of Astrophysics, Bangalore 560034, India*

Accepted 1986 April 29. Received 1986 April 3; in original form 1986 January 27

Summary. The radiative transfer problem in non-LTE moving atmospheres has been explicitly solved for Hα line profiles. These computations have been done for a schematic model of the line-forming region over a wide range of optical depths and velocity gradients in order to cover the observed characteristics in 23 G and K supergiants. The best theoretical fits yield optical depths in the range 10–500 and velocity fields in the range 0.5–3 Doppler widths. The computed mass-flow rates lie in the range 10^{-5}–$10^{-7}\,M_{\odot}\,\mathrm{yr}^{-1}$; the higher the extent of the line-forming region, the lower the mass-loss rates. The effect of the extent on the Hα emission components has also been investigated in some detail. The temperature sensitivity of the mass-loss rates has been considered in an approximate manner.

1 Introduction

Observations over the last decade in particular have generated sufficient evidence that chromospheres of late-type giants and supergiants are expanding (Dupree 1976; Stencel 1978; Stencel & Mullan 1980; Stencel *et al.* 1980). The spectroscopic signatures used extensively in these studies are the Ca II *H* and *K* and Mg II *h* and *k* lines. The central absorption reversal in these lines is believed to be of chromospheric origin in G and K giants and supergiants (Deutsch 1960; Reimers 1975, 1977) and is formed higher in the atmosphere than the emission peaks. An outflow with increasing velocity would then lead to a blueshift in the central core relative to the emission peaks, thereby reducing the flux of the blueward emission relative to that of the red. The presence of this red-dominated asymmetry thus suggests the onset of mass loss in the chromosphere. Wilson (1960) and later Reimers (1981) have inferred from their studies of several giants and supergiants that between one-third and one-half of the terminal velocity is attained in their chromospheres.

In his study of α Ori, Weymann (1962) had noted that the core of the Hα profile was displaced to the blue by a few km s^{-1} with respect to the centre of symmetry of the wings. Like the Ca II triplet in the infrared ($\lambda\lambda$8498, 8542, 8665), it seemed to be forming in a region of the atmosphere uncoupled from the photosphere. Recent observations by Goldberg (1979) confirm that in α Ori, the symmetric cores of the Ca II triplet and Hα are formed in the accelerating wind region,

physically separate from the photosphere but inside the circumstellar (CS) shell. Hartmann (1983) also refers to the above region as the 'extended chromosphere' where the temperatures ($\sim 10^4$ K) and densities ($\sim 10^8$ cm^{-3}) are much higher than in the CS shell and the scale heights are of the order of the stellar radius. Occultation measurements and speckle interferometry also suggest the same (White, Kreidl & Goldberg 1982; Goldberg *et al.* 1982). The free–free emission data of α Ori at several radio frequencies suggest temperatures of 5000–10^4 K, ranging over several stellar radii (Altenhoff, Oster & Wendker 1979; Newell & Hjellming 1982; Wischnewski & Wendker 1981). *IUE* observations of the C II multiplet near 2325 Å in several red giants imply e^- densities $\sim 10^8$ cm^{-3} and scale heights $\sim 1 R_*$ (Stencel *et al.* 1981). Combining these data with C IIλ1335 observations and the measurement of stellar parallaxes and angular diameters, Carpenter, Brown & Stencel (1985) estimated the geometrical extent of the chromospheres of late-type stars to range between 1 and $6 R_*$. The temperatures are found to be in the range 6000–11 000 K. Since the outflow of matter starts in the inner region between the stellar photosphere and the CS shell, the observations of the spectral lines formed there are more effective in providing an understanding of the phenomenon of mass loss in these stars than the study of CS shells where the stellar wind reaches the terminal velocity. And the fact that it reaches almost half of this velocity in the chromosphere itself holds a clue to the mechanism that triggers the flow. The Hα line lies at the red end of the spectrum of cool giants whose stellar continua also peak in the red. Therefore the line is easily observable in these stars. The blueshift of the Hα absorption core is a very good wind signature.

An additional piece of observational data that may lend further information on the chromospheres is the blueshifted and/or redshifted Hα emission lying above the level of continuum. Such emission features were observed in Population II stars (Cohen 1976; Mallia & Pagel 1978) and later in several globular cluster giants (Cacciari & Freeman 1981, 1983). Their origin was then attributed to the expanding CS Shell. Reimers (1981), however, suggested a chromospheric origin for them. Very recently, Dupree, Hartmann & Avrett (1984) have also contended that these emissions may actually be forming in a warm chromosphere and are not the signatures of mass loss. Their model calculations show that the emission arises mainly from regions with sufficient material at high enough temperatures ($\geqslant$7000 K). It is worth exploring how this varies with different physical parameters assumed for the chromosphere.

In an earlier paper, Mallik (1982, hereafter Paper I) had analysed the asymmetries observed in the Hα absorption line in 23 late G and K supergiants. The theoretical Hα profiles were computed using a predetermined line source function obtained by Peraiah (1981) in a treatment of radiative transfer in non-LTE moving atmospheres. Reasonably good fits with the observed line-core displacements and equivalent widths were obtained for Hα optical depths in the range 10–200 and in a region of positive velocity gradients on the order of 1 to 2 Doppler widths (corresponding to 17 to 34 km s^{-1} for a microturbulent velocity of 15 km s^{-1}). Assuming a steady flow, the mass-loss rates were estimated to lie in the range 10^{-6}–$10^{-7} M_\odot$ yr^{-1}. The assumed density variation was a linear decrease with the radial distance in the line-forming region. The equation of continuity was strictly satisfied in the plane-parallel limit which restricted the choice of the extent of the line-forming region to a fraction of the stellar radius.

In the present work the radiative-transfer problem in spherical expanding atmospheres has been explicitly solved to obtain Hα line profiles. It has been assumed that Hα is a photoionization-dominated line and the statistical equilibrium equation for a two-level atom has been used in conjunction with the transfer equation to compute the line-source function and line fluxes in a comoving frame. These have then been transformed to the observer's frame and line profiles have been computed for a variety of optical depths. Since the Hα line forms in a region of positive velocity gradient, the density variation is assumed to be of the form $n(r) \propto r^{-3}$ to satisfy the equation of continuity. The limitation imposed in Paper I on the possible extent of the

line-forming region has thus been removed. The extent of the line-forming region has been taken as a free parameter in the present calculations. The effect of the extent on the emission has been investigated in some detail.

We find in our present analysis that Hα optical depths for all the stars are consistently higher than obtained in the previous analysis (Paper I), by a factor ranging from 3 to 6. The mass-loss rates are also higher by more than an order of magnitude. The strength of the Hα emission does increase with the extent of the line-forming region at a given optical depth, though not very strongly owing to dilution effects. Section 2 gives the observational data. Section 3 describes the theoretical framework for the analysis of the line profiles and also the results obtained from this analysis. Conclusions are given in Section 4.

2 Observational data

Hα observations of 23 late-type supergiants described in Paper I are used in our present analysis. Basic data for the stars are given in table 1 of Paper I. Spectra of these stars were obtained with an echelle spectrograph at the coudé focus of the 40-inch telescope at Kavalur Observatory using a 7-inch camera and an uncooled single-stage Varo image intensifier. The dispersion in the 34th order where Hα appeared was $\sim$10.5 Å mm^{-1}. The Hα profile was always seen to be asymmetric in the sense that the absorption core was shifted to the blue with respect to the line centre. The equivalent width (EQW) and the line core displacement (LCD) of the Hα absorption line are listed for all the stars in Table 2 of the present paper. Spectra obtained for 13 out of the 23 stars were fully widened along the slit, thereby giving a better signal-to-noise ratio. In these stars, therefore, it was possible to detect the small emission component of Hα lying above the level of the continuum. The strength of this emission for the 13 stars is given in Table 1 below. The letters '*r*' and '*b*' denote respectively the red and the blue ends of the Hα absorption where the emission appears. For four of the stars, it appears on the red side and for the remainder on the blue side.

Table 1. Hα emission strengths.

Star	Spectral type	EQW of Hα emission (Å)
ϵ Gem	G8Ib	0.09 b
ζ Cep	K1Ib	0.12 b
ϵ Peg	K2Ib	0.11 b
η Per	K3Ib	0.09 r
o^1 CMa	K3Iab	0.07 b
HD 56577	K3Ib	0.09 b
HD 68553	K3Ib	0.04 r
HD 80108	K3Ib	0.09 r
HD 4817	K5Ib	0.05 b
λ Vel	K5Ib	0.13 b
ξ Cyg	K5Ib	0.13 b
σ CMa	K7Iab	0.09 b
HD 216946	M0Ib	0.15 b

Hα observations of red giants in globular clusters (Cohen 1976; Mallia & Pagel 1978; Reimers 1981; Cacciari & Freeman 1981) have also shown that the emission component frequently lies on both sides of the deep absorption profile and in some cases appears either on the blue or on the red side. Moreover, these emission components are not constant in time and their strengths may vary significantly over a few days. For example, Cacciari & Freeman (1983) observed the star 65 in ω Cen that showed stronger emission in the red than in the blue; five days later, the situation was reversed. One month later, the emission was quite strong on both sides and became very weak on both the sides after another month. They also reported observations of the star A31 in NGC 6752 which showed strong red and blue emission and a month later had only red emission. In view of these observations of the Hα variability over short time-scales, it must be emphasized here that for our programme stars, though the emission component at any one time was unambiguously detected only on one side, the possibility of its being there on the other side simultaneously or at another time is not totally ruled out. It should also be remembered that the question of variability was not investigated.

3 Analysis of line profiles

3.1 THEORETICAL FRAMEWORK

Because of the vast geometrical extent of the supergiants and the outward flow of matter from these stars, it is only proper to treat the radiative-transfer problem in the framework of extended expanding non-LTE atmospheres. Kunasz & Hummer (1974) studied line formation in optically thick systems with radial gas flow in the observer's frame. In this frame, when the outflow velocity exceeds 2 or 3 thermal units, the frequency-angle mesh becomes very large and difficult to handle particularly for large optical depths. In the comoving frame, no relative velocities exist, so only a small number of frequencies need be considered. Moreover, in the latter case, the angle-averaged redistribution function is adequate, as opposed to the observer's frame calculations where the full redistribution function should be used. Detailed comoving frame calculations have been performed by Mihalas, Kunasz & Hummer (1975). For our purpose, we have used the comoving frame radiative-transfer code developed by Peraiah (1980a, b, 1981) which is based on the discrete space theory of Grant & Peraiah (1972). The equation of line transfer in the comoving frame is given by

$$\pm\mu\frac{\partial I(x,\pm\mu,r)}{\partial r}\pm\frac{1-\mu^2}{r}\frac{\partial I(x,\pm\mu,r)}{\partial\mu}$$
$$=k_l[\beta+\phi(x)][S(x,r)-I(x,\pm\mu,r)]+\left\{(1-\mu^2)\frac{V(r)}{r}+\mu^2\frac{dV(r)}{dr}\right\}\frac{\partial I(x,\pm\mu,r)}{\partial x}. \quad (1)$$

± denote respectively the outgoing and incoming beams. $I(x, \pm\mu, r)$ is the specific intensity making an angle $\cos^{-1}\mu$ with the radius vector at the radial point for the frequency x where $x=\nu-\nu_0/\Delta\nu_D$, $\Delta\nu_D$ being the Doppler width and $V(r)$ the velocity of the gas at the radial point r in Doppler widths. The function $\phi(x)$ is the line-profile function. For calculating Hα line profiles, we assume a two-level atom. The justification for this lies in the fact that temperatures prevailing in the chromospheres of G and K supergiants are in the range 4000–8000 K for which the Lyman continuum and Lyman lines are optically thick and thus the levels 1 and 2 of hydrogen approach radiative detailed balance (Jefferies & Thomas 1959). $S(x, r)$ is the source function given by

$$S(x,r)=\frac{\phi(x)}{\beta+\phi(x)}S_l(r)+\frac{\beta}{\beta+\phi(x)}S_c(r),$$

$S_l(r)$ and $S_c(r)$ denoting the line and the continuum source functions; β is k_c/k_l where k_c and k_l are the continuum and the line-absorption coefficients. $S_c(r)$ is usually taken as the Planck function and $S_l(r)$ is given by

$$S_l(r)=\frac{1-\varepsilon}{\phi(x)}\int_{-\infty}^{\infty}dx'\int_{-1}^{1}I(x',\mu',r')\,R(x,x')\,d\mu'+\varepsilon B(r), \tag{2}$$

where $R(x, x')$ is the angle-averaged redistribution function and ε the photon destruction probability by collisional de-excitation.

The optical depth in a line is given by

$$\tau=\frac{\sqrt{\pi}e^2}{mc}\frac{f}{\Delta\nu_D}N, \tag{3}$$

where f is the oscillator strength of the transition. N can be written as

$$N=\int_{R_{in}}^{R_{out}}n\,dr$$

where n is the number density of the line-forming atoms distributed over the extent of the line-forming region $\Delta R=R_{out}-R_{in}$.

In the discrete space theory, the variables x, μ, r in the equations (1) and (2) are discretized. The integrals are approximated by the appropriate quadrature sums and the differentials by the weighted differences. The integration over angle and frequency variables is effected by the quadrature formula where the total number of angles and frequencies is specified. The extent ΔR is divided into a discrete number of shells. The equation then is cast in a matrix form so that a comparison with the interaction principle gives the reflection (r) and transmission (t) matrices and source vectors in each shell (Peraiah 1980a). One can then calculate the diffuse radiation field and the source functions by employing the scheme of Internal Field (Peraiah & Grant 1973) and calculating the r and t matrices.

The basic quantity obtained from the solution of the transfer equation is the dependence on depth of the line-source function. With the line-source function thus known from the comoving-frame calculations, the emergent flux as a function of frequency is calculated from a formal solution of the observer's frame transfer equation for a variety of strengths. These computed line profiles are then used for comparison with observations.

3.2 MODEL ADOPTED

Since the bulk of the Hα absorption forms in the chromosphere, the inner radius R_{in} is taken to be the stellar photospheric radius $R_*=R_{in}$, around the region of temperature minimum. The outer radius is used as a free parameter in the line-profile calculations, ranging between 1.1 R_* and 6R_*. Since the blueshift of the absorption core causing the asymmetry in the observed profiles strongly suggests a differentially expanding gas, the velocity distribution is assumed to be linearly increasing outward with V_{out} ranging from 1 to 6 $\Delta\nu_D$'s. To conserve mass flux, the density distribution (which in turn reflects the depth dependence of opacity) then varies as r^{-3}. Since the line opacity of Hα is rather large, β is approximated to zero. It is also assumed that Hα is a photoionization-dominated line and ε is set to zero. This situation corresponds to pure scattering in the medium. The profile function $\phi(x)$ is assumed to be a pure Doppler function since Doppler broadening dominates the Hα profile. In that case, complete redistribution of photons holds good, i.e. $R(x', x)=\phi(x')\,\phi(x)$ which reduces the line-source function to

$$S_l(r)=\int_{-\infty}^{\infty}\phi(x')\,dx'\int_{-1}^{+1}I(x',\mu',r)\,d\mu'. \tag{4}$$

As mentioned earlier, one does not have to take a large number of frequency and angle points in a comoving frame. The program was tested by Peraiah (1981) for several sets of frequency and angle points and source functions were computed for each set. It was found that these are quite insensitive to the number of frequency-angle points. We have chosen a grid of two angles and nine frequency points for our purpose. Test calculations show this to be quite adequate for small velocities.

We impose two boundary conditions on our problem. The first is that the radiation incident from the inside of the atmosphere is the Planck field $B(r)$ which we parameterize to unity and that from the outside is zero. The second is that the frequency derivative term appearing in the transfer equation is zero. This is equivalent to satisfying the condition of flux conservation in a pure scattering medium.

The total integrated line optical depth needs to be specified for each run. $\Delta\nu_D$ in (3) contains a term for microturbulence in addition to the thermal term. The root mean square turbulence ξ_t is suspected to be quite large in supergiants particularly in the chromospheres (Kuhi 1974; Boesgaard & Hagen 1979; Ayres & Linsky 1975). Hartmann, Dupree & Raymond (1981) found extremely wide lines from a high dispersion *IUE* study of α *TrA* implying large non-thermal motions. Ayres *et al.* (1982) found similarly large linewidths. Hartmann & MacGregor's (1980) wind model also predicts a large line-of-sight turbulent velocity $\sim 25\,\mathrm{km\,s^{-1}}$ for a density $\sim 10^8\,\mathrm{cm^{-3}}$ characteristic of extended chromospheres. We assume a more modest value of $15\,\mathrm{km\,s^{-1}}$ in our line-profile calculations. The other unknown term in τ is the population in level $n=2$ of H. The temperature rise in the chromosphere resulting in the observed large strength of Hα has to be simulated as a first approximation, by choosing an average temperature higher than the LTE excitation temperature. Basri (1979), Basri & Linsky (1979) and Basri, Linsky & Eriksson (1981) have built chromospheric models of late-type supergiants, β Dra, ε Gem and α Ori. These models fit very well the observed Ca II *H* and *K* and Mg II *h* and *k* fluxes. The models give a run of temperature, density, microturbulent velocity versus the geometrical height. Their model of ε Gem (one of our programme stars) gives, for chromospheric densities $\sim 10^8\,\mathrm{cm^{-3}}$, a microturbulent velocity of $\sim 12\,\mathrm{km\,s^{-1}}$ and a temperature of 6000 K. We have assumed a temperature of 6000 K for the Hα forming region. The optical depth thus calculated is used as a parameter in the computations.

The optical depth and the geometrical depth in each shell are chosen such that stable, unique and positive solutions are obtained. The r and t matrices should be positive implying that the diagonal elements of curvature matrices should be positive and the off-diagonal elements negative. These conditions impose a restriction on τ in each shell such that $\tau_{\mathrm{shell}} < \tau_{\mathrm{crit}}$ the expression of which is given in Peraiah (1981). τ_{crit} depends, in particular, upon the curvature factor $\Delta r/R_{\mathrm{out}} - R_{\mathrm{in}}$ (where Δr is the geometrical depth in each shell), the velocity of the medium and the differential velocity. The other criterion for the positivity of fluxes is that $\Delta r/\tau$ should be very small ($\sim 10^{-3}$). In order to use the computer time and the storage capacity within reasonable limits, we have restricted the number of shells to 20. Since we are dealing with large optical depths, each shell has been further subdivided so that τ in each sub-shell is less than τ_{crit} – the criterion on the positivity of fluxes. During the course of our calculations, we did encounter a few profiles with low τ and high V_{out} that gave negative fluxes at one or two frequency points and therefore rejected them.

3.3 RADIATIVE-TRANSFER SOLUTIONS AND COMPUTATION OF Hα LINE FLUXES

The program was subjected to two tests. The first one was to check the flux conservation in a scattering medium ($\varepsilon=0$, $\beta=0$). The second one was to compute the intensities in a pure absorbing medium ($\varepsilon=1$, $\beta=0$) for which an analytical solution exists. Once the program was

checked for these tests, the Hα source functions and the corresponding emergent fluxes were computed for a range of optical depths. For a given choice of optical depth, the most important remaining parameters are ΔR and V_{out}.

A few representative Hα source functions are displayed in Fig. 1 as a function of optical depth. It is seen that for the scattering medium approximation, the source function falls in the outward direction by two to three orders of magnitude. For higher ΔR and for a given τ and V_{out} the fall is steeper, almost four to five orders of magnitude. For higher V_{out} the drop is steeper for a given τ and ΔR. These trends are understandable since, for large velocity gradients and for a very extended atmosphere, there is a greater probability of a photon being scattered from the core to the wing and hence of its escaping. For each source function thus obtained for a given τ, V_{out} and ΔR, the Hα line profile is computed in the comoving frame and transformed into the observer's frame. This is repeated for a range of parameters $10 \leqslant \tau \leqslant 1000$, $\Delta v_D \leqslant V_{out} \leqslant 6\Delta v_D$ and $0.1 R_* \leqslant \Delta R \leqslant 5.0 R_*$.

For a source function of the above form, the resultant line profile is basically a strong absorption profile having a deep core shifted to the blue with respect to the line centre and a small emission lying to the red of the absorption profile. A few representative Hα line profiles are shown in Fig. 2. For a given extent, the strength of the absorption and also the depth of the core increase with the integrated optical depth at a given velocity gradient. The velocity gradient increases the strength of the line at a given optical depth. It also tends to desaturate the line core. The line core shift increases with increasing flow velocity. It also increases monotonically with τ as stronger lines saturate farther and farther out in the flow and sample larger flow velocities. In an

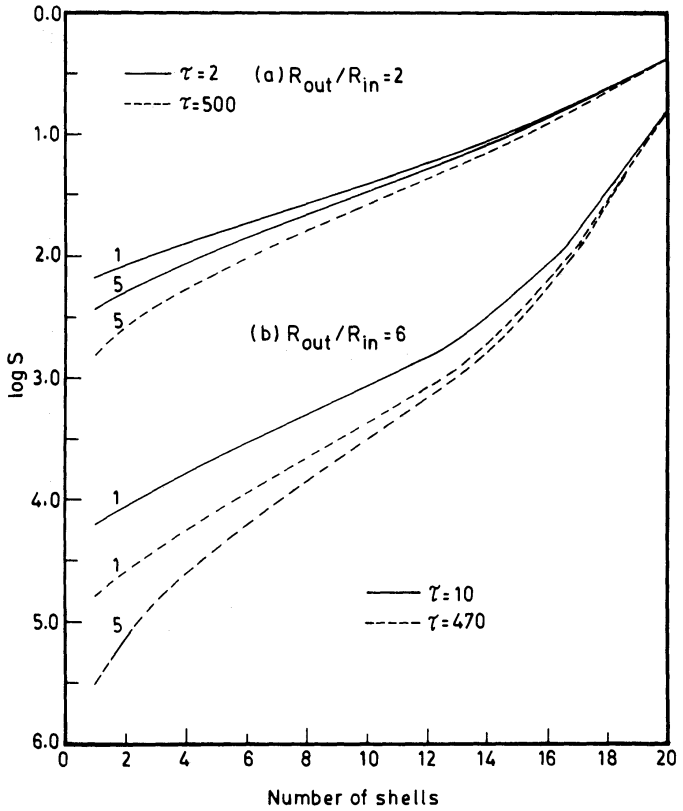

Figure 1. Frequency independent source functions for $\varepsilon=0, \beta=0$ plotted against the number of shells (which is a function of optical depth) for (a) $R_{out}/R_{in}=2$ and (b) $R_{out}/R_{in}=6$. The number denoted for each curve is the velocity at R_{out} in Doppler units.

expanding atmosphere with a velocity increasing outward, lines tend to be skewed towards shorter wavelengths (Mihalas 1979).

The lobes on either side of the absorbing column emit photons thermally or scatter them from both the stellar and diffuse radiation fields. The velocities along the line-of-sight in the lobe material range from positive to negative values and produce an emission feature extending from a wavelength to the violet of the rest wavelength to redder wavelengths (Mihalas 1978). This emission is superposed in the underlying absorption feature, the net effect being a red emission lying above the level of the continuum. The bigger the emission lobes are, the more the emission should be. It is seen in the present computations that this is generally true, although, at a given τ, the emission does not increase in proportion to the extent because the same amount of matter is distributed over a larger volume, and because of the dilution effect, not enough radiation is present at larger distance to be scattered.

All the above computations are for a pure scattering medium. Computations have also been carried out for a non-zero $\varepsilon(\varepsilon=10^{-3})$ for two optical depths and a range of velocity gradients and for $\Delta R=10^{13}$ cm. It is seen that a non-zero ε tends to lift the core. Moreover, the emission strengths also increase with increasing ε. For a given ε, linewidths always increase with increasing line strength, velocity gradient and microturbulence.

3.4 OPTICAL DEPTHS, VELOCITIES AND MASS-LOSS RATES

Limitations set by the medium resolution of the spectra ($\sim 3\times10^4$) did not permit us to do a point-to-point matching of the theoretical profiles with the observed. Only the gross features of

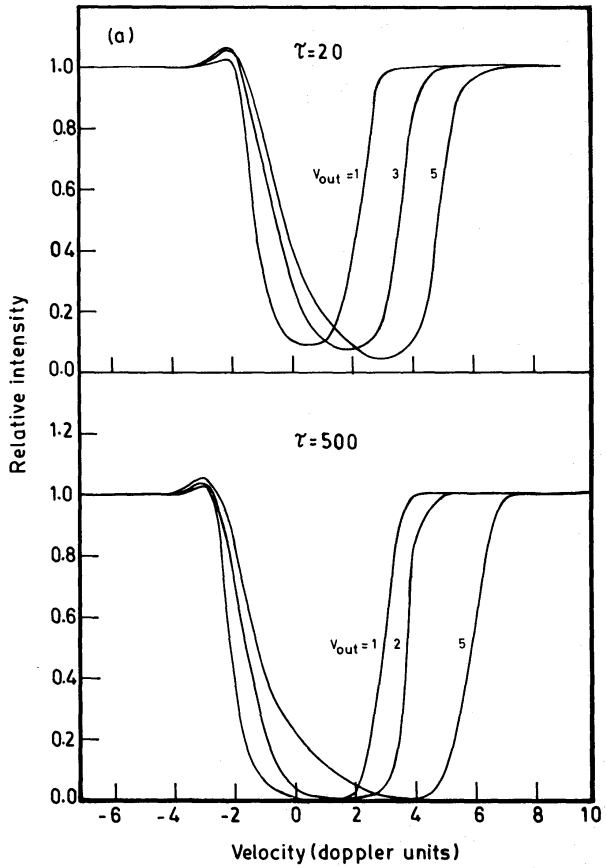

Figure 2. Computed Hα profiles for (a) $R_{out}/R_{in}=1.1$ for $\tau=20$ and 500, (b) $R_{out}/R_{in}=2$ for $\tau=10$ and 240 and (c) $R_{out}/R_{in}=6$ for $\tau=30$ and 470. The number denoted for each curve is the outer velocity V_{out} in Doppler units.

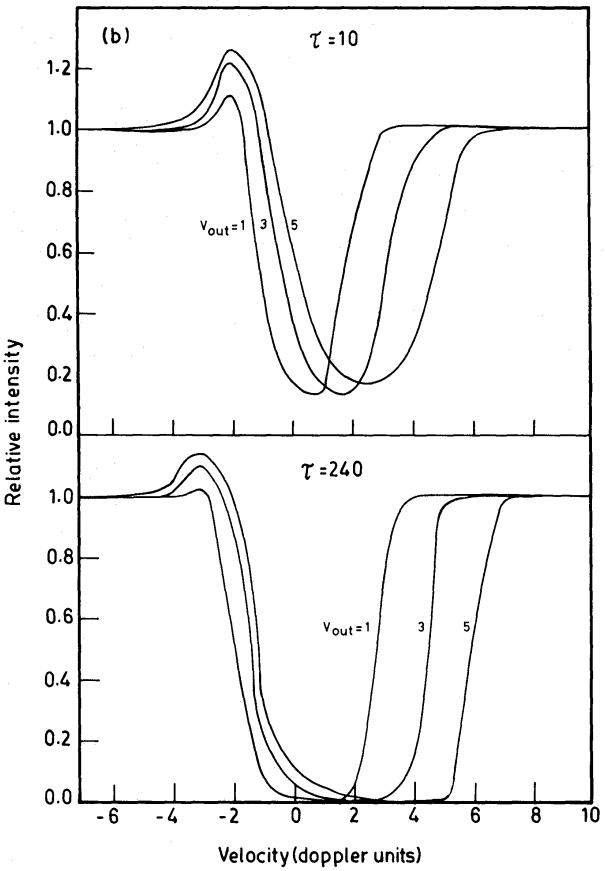

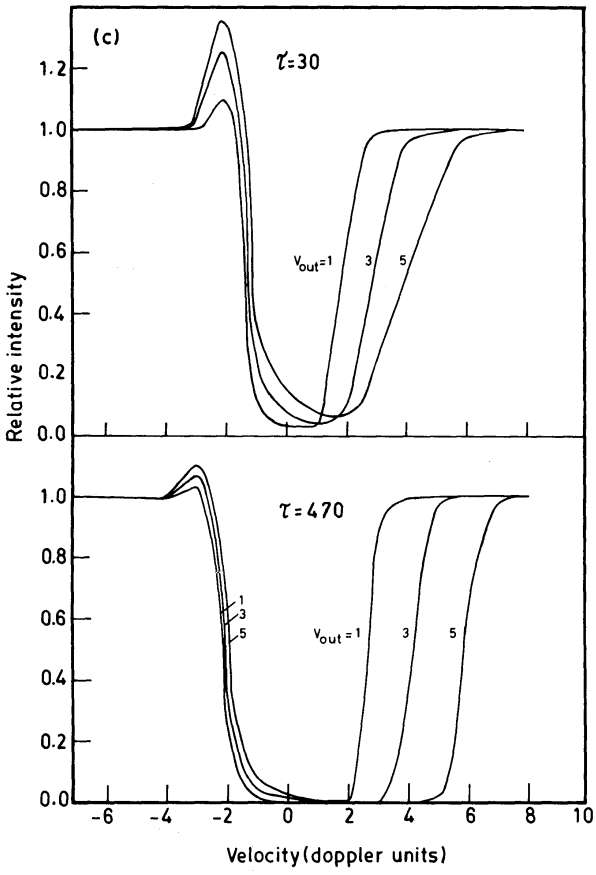

Figure 2–*continued*

the line, namely, the EQW and the LCD were investigated. These were determined for all the theoretical Hα absorption profiles. In the light of the objections raised by Reimers (1981) and Dupree *et al.* (1984) to the origin of the Hα emission in the CS shell, no attempt has been made to derive mass-loss rates from the emission components. According to them, the emission can originate even in non-moving deep chromospheric layers and the true wind signature is the blueshift of the overlying absorption and the apparent blueshift of the core. Therefore, to obtain the optical depths, velocity fields and the mass-loss rates in the expanding line-forming regions for a given ΔR, the procedure described in detail in Paper I was adopted. The plots of theoretical EQW versus τ for each V_{out} and of theoretical LCD versus V_{out} for each τ for the extent $\Delta R = 5\times10^{13}$ cm are displayed in Fig. 3. The (τ, V_{out}) solutions were obtained by matching the observed EQW and LCD with the theoretical. The optical depth and the outer velocity thus

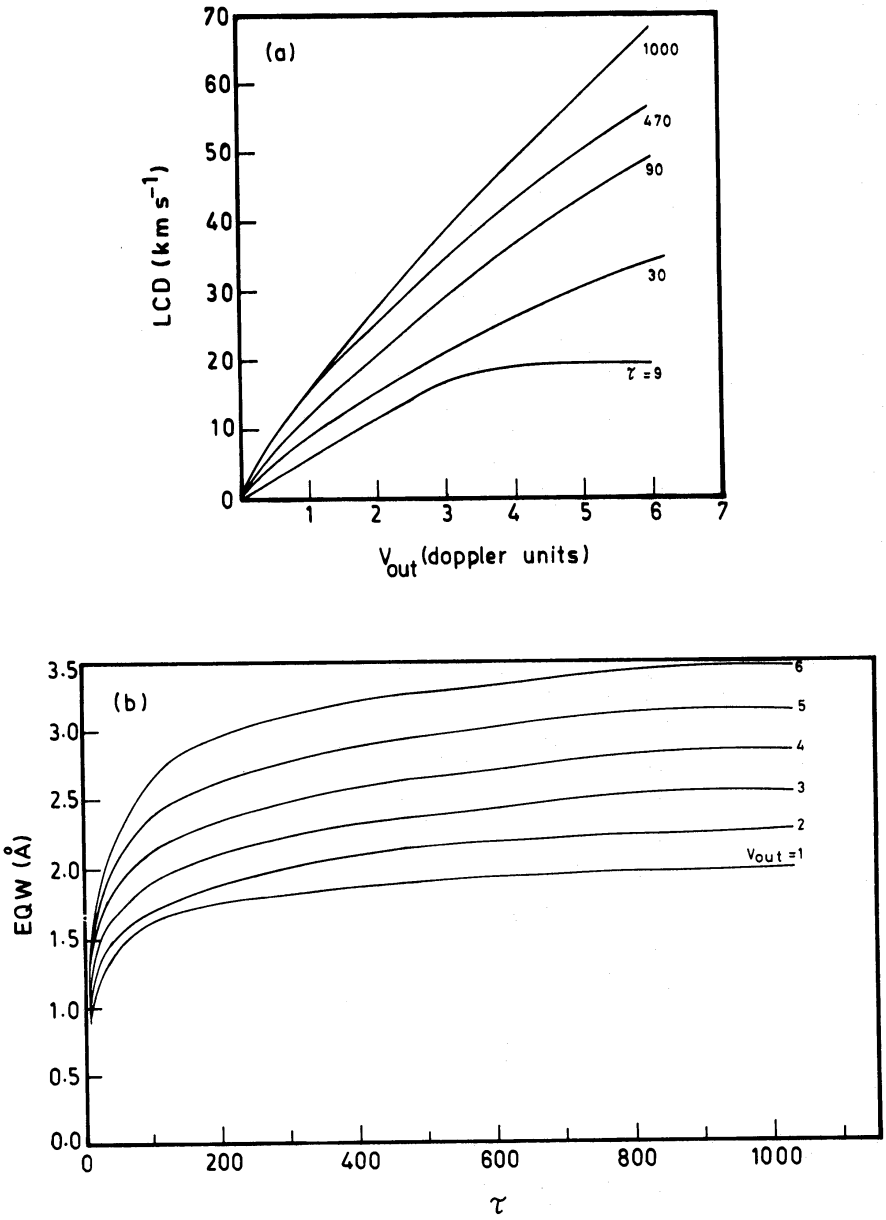

Figure 3. (a) The computed line-core displacement versus outer velocity for $R_{out}/R_{in}=6$. Each curve is labelled by the optical depth τ. (b) The computed equivalent width versus optical depth for $R_{out}/R_{in}=6$. Each curve is labelled by the outer velocity V_{out}.

obtained for each star are displayed in Table 2. These optical depths are higher than those obtained in the previous analysis (Paper I) by a factor of 3 to 6. The rate of mass ouflow from the atmosphere assuming the steady flow condition can be calculated from the equation

$$\dot{M}=4\pi r^2\varrho(r)\,V(r) \tag{5}$$

where $4\pi r^2$ is the surface area through which the matter is moving. We need to know the density $\varrho(r)$, the outflow velocity $V(r)$ and the position (i.e. the surface area covered) of the gas at which we are looking. None of the methods determining the mass-loss rates tell us all the three without assuming several model-dependent parameters (Goldberg 1979; Castor 1981; Trimble 1984). In the present context, when the above equation is expressed in terms of observable quantities, the important parameters that figure are the state of excitation of hydrogen (the level $n=2$ population), the inner radius, the temperature and density as a function of radius above the stellar photosphere and microturbulence. It implicitly assumes the absence of inflow and non-radial motions. Equation (5) can be rewritten as

$$\dot{M}=4\pi r^2(1+\eta)\,m_{\rm H}n(r)\,V(r). \tag{6}$$

On the basis of the choices already made of the various parameters, mass-loss rates are evaluated at the outer radius where $V(r)=V_{\rm out}$, $r=R_{\rm out}$ and $n(r)$ is the density at the outer radius. The determination of mass-loss rates is repeated for all the values of $R_{\rm out}$ chosen in the line-profile calculations. These are displayed in Table 2. $R_{\rm in}$ was assumed to be 10^{13} cm in conformity with what Luck (1978) obtained for G and K supergiants. The mass-loss rates are systematically lower for higher ΔR. For the range of extents from 10^{12} cm to 5×10^{13} cm, the mass-loss rates differ by almost the same factor. They are consistently higher by more than an order of magnitude than obtained in the earlier analysis (Paper I). The spherical calculations show that the equivalent width of the profile grows more slowly with optical depth than in the plane-parallel case. Hence, for a given observed equivalent width, a higher τ is inferred in the spherical case which, in turn, implies a higher density and a higher mass-loss rate. Without an independent determination of the extent of the line-forming region, it is not possible to pinpoint the exact magnitude of the mass-loss rate. It is worth noting that for the range of optical depths and velocity gradients tried, the computed emission strengths for the extents $0.1\,R_*$ and $0.5\,R_*$ are too small; much smaller than observed in the program stars where it ranges between 10 and 100 m Å. The computed profiles that reproduce the observed absorption and the blue displacement and also match the strength of the redward emission of the program stars correspond to values of $\Delta R\geqslant 1\,R_*$. Thus we conclude that the observed characteristics of the Hα line are reproduced only if the chromosphere extends at least as much as the stellar radius.

The mass-loss rate estimates assume an average temperature of 6000 K in the chromosphere. It is important to realize that this rate is sensitive to temperature since it is directly proportional to the population in the hydrogen level 2. It is possible to obtain an idea of the temperature sensitivity of the mass-loss rates in an approximate manner which is also consistent with the assumptions that have already gone into the transfer calculations. Thus, since Lyα and Lyβ are in detailed balance, and if we also neglect the transfer in Hα, the $n=2$ population is determined by the balance between photoionization out of the Balmer continuum and recombination to the $n=2$ level of hydrogen. Following Hartmann & MacGregor (1980), the photoionization rate from the $n=2$ level can be written as

$$\beta_2=\frac{8\pi W}{h^3c^2}\sigma_{20}I_2^3E_1(I_2/kT_{\rm R})$$

where W is the dilution factor, I_2, the ionization potential from level 2, σ_{20}, the threshold

Table 2. Optical depths, velocity fields and mass-loss rates.

			$R_{out}/R_{in}=1.1$				$R_{out}/R_{in}=2$				$R_{out}/R_{in}=6$			
Star	EQW (Å)	LCD ($kmsec^{-1}$)	V_{out} ($kmsec^{-1}$)	τ	$n_o(10^{11})$ (cm^{-3})	$M/M_\odot$ (yr^{-1})	V_{out} ($kmsec^{-1}$)	τ	$n_o(10^{10})$ (cm^{-3})	$M/M_\odot$ (yr^{-1})	V_{out} ($kmsec^{-1}$)	τ	$n_o(10^{10})$ (cm^{-3})	$M/M_\odot$ (yr^{-1})
ϵ Gem	1.77	- 8.1	10.7	290.	30.	4.67(-5)	9.7	260.	59.	4.61(-6)	9.4	225.	32.5	8.16(-7)
HD77912	1.33	-13.4	20.5	35.	3.8	1.12(-5)	17.7	35.	7.5	1.07(-6)	29.9	25.	3.5	2.80(-7)
33 Sgr	1.67	- 4.9	6.4	175.	18.5	1.73(-5)	5.6	172.5	39.5	1.79(-6)	5.1	125.	18.	2.47(-7)
ζ Cep	1.81	-13.8	19.2	320.	33.5	9.38(-5)	17.1	285.	65.	8.91(-6)	17.1	275.	40.	1.83(-6)
HD196093	1.34	-18.6	28.1	35.	3.8	1.54(-5)	25.1	35.	7.5	1.51(-6)	53.7	17.5	2.5	3.60(-7)
ϵ Peg	1.80	- 8.7	11.9	320.	33.5	5.84(-5)	10.7	285.	65.	5.61(-6)	10.2	275.	40.	1.10(-6)
γ Per	1.84	- 7.5	10.2	395.	41.3	6.16(-5)	9.0	360.	82.	5.95(-6)	8.5	380.	55.	1.26(-6)
HD17958	1.27	-17.2	26.4	25.	2.8	1.06(-5)	23.4	25.	5.5	1.03(-6)	46.1	15.	2.	2.47(-7)
o^1 CMa	1.22	- 6.9	10.2	25.	28.	4.11(-6)	8.9	22.5	4.5	3.21(-7)	17.1	27.5	4.	1.83(-7)
41 Gem	1.36	- 9.2	13.6	40.	4.3	8.47(-6)	11.8	35.	7.5	7.09(-7)	17.1	40.	5.5	2.51(-7)
HD56577	1.47	- 6.1	9.0	58.	6.5	8.50(-6)	7.2	70.	16.	9.21(-7)	9.4	60.	8.5	2.14(-7)
HD62576	1.23	-15.4	23.9	25.	2.8	9.59(-6)	20.5	22.5	4.5	7.40(-7)	40.9	17.5	2.5	2.74(-7)
HD68853	1.51	-30.1	46.9	25.	2.8	1.88(-5)	46.9	30.	6.5	2.23(-6)	85.3	10.	1.5	3.43(-7)
HD80108	1.68	-21.4	30.7	100.	10.5	4.71(-5)	31.4	60.	13.5	3.40(-6)	44.4	70.	10.	1.19(-7)
HD91056	1.98	- 8.7	11.9	750.	78.3	1.36(-4)	10.7	600.	137.5	1.19(-5)	8.5	950.	138.	3.15(-6)
β Ara	1.60	-18.3	27.3	60.	6.5	2.59(-5)	24.4	47.5	10.5	2.06(-6)	35.8	65.	9.	8.63(-7)
HD4817	1.81	-12.0	16.2	320.	33.5	7.92(-5)	14.8	285.	65.	1.75(-6)	14.5	275.	40.	1.55(-6)
λ Vel	1.66	-11.8	15.8	175.	18.5	4.26(-5)	14.5	150.	34.	3.96(-6)	17.1	110.	16.	7.31(-7)
HD89388	1.79	-22.9	32.4	200.	21.	9.94(-5)	29.0	117.5	26.5	6.17(-6)	47.8	75.	10.5	1.34(-6)
HD137709	1.69	- 9.3	12.4	220.	23.	4.15(-5)	11.4	190.	43.5	3.99(-6)	11.9	140.	20.	6.39(-7)
ζ Cyg	1.93	- 9.3	12.4	525.	55.	9.93(-5)	11.4	475.	109.	1.00(-5)	8.5	600.	87.	1.99(-6)
σ CMa	1.72	-10.6	14.1	240.	35.	5.14(-5)	12.8	210.	48.	4.93(-6)	13.6	160.	23.	8.40(-7)
HD216946	1.83	-17.1	23.5	350.	36.5	1.25(-4)	20.8	320.	73.	1.22(-5)	20.5	340.	49.	2.68(-6)

cross-section, T_R, the characteristic radiation temperature and E_1 is the first exponential integral. Similarly, the recombination rate is given by

$$\alpha_2 = \frac{8\pi\sigma_{20}}{c^2} \frac{4I_2^3}{(2\pi mkT)^{3/2}} \exp(-I_2/kT)\, E_1(I_2/kT).$$

Ionization equilibrium then requires

$$n_2 = \frac{8n_H\, U_+/U_0 \exp(-I_1/kT) \exp(-I_2/kT)\, E_1(I_2/kT)}{W E_1(I_2/kT_R)}$$

where U_+/U_0 is the ratio of partition functions and equals ½ for hydrogen. I_1 is the ionization potential from level 1. $W = ½$ at the surface. Then

$$n_2 = \frac{8n_H \exp(-I_1/kT) \exp(-I_2/kT)\, E_1(I_2/kT)}{E_1(I_2/kT_R)}. \tag{7}$$

For cool supergiants of effective temperature ~4250 K, the radiation temperature can be approximated as

$T_R = 3800$ K for $T \geqslant 6000$ K

$T_R = 3800 + 1.6(T - 6000), 6000 \leqslant T \leqslant 8000$ (see Hartmann & MacGregor 1980).

Equation (7) gives the approximate temperature and density dependence of the $n=2$ population. Since the Hα absorption occurs in a situation of pure scattering, the important parameter is the optical depth, which is directly proportional to the $n=2$ population. Thus for a specific radiative-transfer solution, equation (7) can now be used to infer the change in density required to get the same $n=2$ population as the temperature is changed. This exercise has been performed for temperatures varying between 4500 and 8000 K – a plausible range for the stars under study. The variation in the mass-loss rate estimate as a function of temperature is shown in Fig. 4. In the range 5000–8000 K, the mass-loss rates vary by a factor of ~10^3, being lower for higher temperatures.

4 Conclusions

Hα line profiles have been calculated by solving for the source function in the comoving fluid frame and computing emergent intensities using a formal solution in the observer's frame.

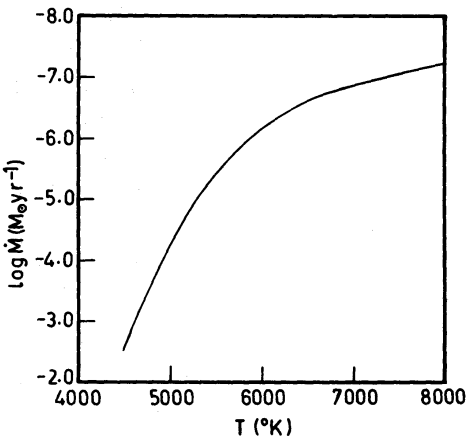

Figure 4. The change in the mass-loss rate with temperature.

Computations have been done for a schematic model of the line-forming region over a wide range of τ and V_{out} which cover the observed characteristics in 23 G and K supergiants. From the computed emergent flux profiles, parameters describing their width and shape have been obtained. The computed profiles that fit the observations in the sense of reproducing the deep absorption and small blue asymmetries yield optical depths in the range 10–500 and velocity fields in the order 0.5 to 3 Doppler widths implying velocity gradient of 10 to 40 km s^{-1} for microturbulent velocities of 15 km s^{-1}. The mass-flow rates lie in the range 10^{-5}–$10^{-7}\,M_{\odot}\,yr^{-1}$ for the thickness of the chromospheres ranging between 10^{12} cm and 5×10^{13} cm. Considering the number of free parameters involved in the determination of the mass-loss rates, the above method yields at best an order of magnitude estimate. Nevertheless, these values seem to be rather large, partly owing to the high chromospheric densities. The expanding region is of course gravitationally bound to the star, since the surface escape velocity for a supergiant of $10\,M_{\odot}$ at a distance of $5\,R_{*}$ is approximately 50 km s^{-1}, larger than the flow velocities inferred here. A more basic question is whether the observed asymmetries can be uniquely interpreted as the differential expansion due to mass-loss (Hartmann 1983; Linsky 1980; Baliunas 1983). Hummer & Rybicki (1968) have demonstrated that a differentially expanding atmosphere can produce line asymmetries. However, asymmetries can at most provide information on velocity gradients (Athay 1970; Cram 1972) but not necessarily on the magnitude or the direction of the flow. Mihalas (1979) has shown that by a careful and systematic study of the parameters for a range of line strengths, it is possible to determine the representative velocity field with some accuracy though the results remain model-dependent.

Very recently, Cram & Mullan (1985) have studied the problem of Hα formation in the chromospheres of cool stars and shown that the great widths of the Hα absorption lines observed in these stars are due to non-thermal chromospheric velocity fields. They emphasize that despite Hα being a photoionization-dominated line, its line profile does respond to changes in chromospheric structure. There is an intimate coupling between the chromospheric optical thickness, absorption profile, the non-LTE line-source function and the assumed radiation field incident from the photosphere on to the chromosphere.

There are several limitations of our model. The most serious of all is the state of excitation of H, i.e. the $n=2$ population. This is amply demonstrated by the strong temperature sensitivity of the mass-loss rates (Fig. 4). It is very important to understand the exact mechanism of Hα formation in the expanding supergiant chromospheres. A proper and complete treatment of the Hα line transfer would involve statistical equilibrium equations for a multi-level atom (number of levels $\geqslant$3), as well as assumptions regarding the run of temperature and microturbulent velocity with depth, inclusion of the partial redistribution effects and finally solving the equation of radiative transfer with all these inputs. The problem is enormously complicated and the computing requirements are nearly prohibitive. However, a beginning has been made by considering first a more realistic model of the Hα excitation (a five-level H atom). Calculations are in progress.

As discussed earlier, the Hα emission wings observed in G and K supergiants are now believed to originate in a warm, not necessarily expanding chromosphere and not in the CS envelope. Semi-empirical chromospheric models have been computed for both normal-abundance stars and metal-deficient giants (Baliunas *et al.* 1979; Dupree, Hartmann & Avrett 1984; Dupree, Avrett, Hartmann & Smith 1984) showing that emission wings on either side or both the sides of the Hα absorption profile can be produced in a static or expanding chromosphere with a steep temperature gradient. These authors find that it is necessary to have sufficient material at high temperatures (~8000 K) in the outer chromosphere to produce the emission in the wings. In their calculations, the redward emission is generally found to be more than the blueward emission. Our computations assume a constant and not so high temperature across the atmosphere and give emission only on the red side of the overlying absorption. This emission is a direct consequence of

the optically thin extended lobes around the star, similar to that found in a typical P-Cygni profile. It is worth attempting a realistic model calculation with a definite temperature structure to see if emission wings similar to what Dupree *et al.* (1984) find are produced. This problem will be addressed in a future paper.

Acknowledgments

I am grateful to Professor A. Peraiah for letting me use his radiative transfer code. I especially express my sincere thanks to K. E. Rangarajan and D. Mohan Rao for all their help in the computations. I am indebted to the referee for extremely helpful suggestions. I also thank D. C. V. Mallik for a critical reading of the manuscript.

References

Altenhoff, W. J., Oster, L. & Wendker, H. J., 1979. *Astr. Astrophys.*, **73,** L21.
Athay, R. C., 1970. *Sol. Phys.*, **11,** 347.
Ayres, T. R. & Linsky, J. L., 1975. *Astrophys. J.*, **200,** 660.
Ayres, T. R., Linsky, J. L., Basri, G. S., Landsman, W., Henry, R. C., Moos, H. W. & Stencel, R. E., 1982. *Astrophys. J.*, **256,** 500.
Baliunas, S. L., 1983. *Publs astr. Soc. Pacif.*, **95,** 532.
Baliunas, S. L., Avrett, E. H., Hartmann, L. & Dupree, A. K., 1979. *Astrophys. J.*, **233,** L129.
Basri, G. S., 1979. *PhD thesis*, University of Colorado, Boulder, Colorado.
Basri, G. S. & Linsky, J. L., 1979. *Astrophys. J.*, **234,** 1023.
Basri, G. S., Linsky, J. L. & Eriksson, K., 1981. *Astrophys. J.*, **251,** 162.
Boesgaard, A. M. & Hagen, W., 1979. *Astrophys. J.*, **231,** 128.
Cacciari, C. & Freeman, K. C., 1981. In: *Physical Processes in Red Giants,* p. 311, eds Iben, I. Jr & Renzini, A., Reidel, Dordrecht, Holland.
Cacciari, C. & Freeman, K. C., 1983. *Astrophys. J.*, **268,** 185.
Carpenter, K. G., Brown, A. & Stencel, R. E., 1985. *Astrophys. J.*, **289,** 676.
Castor, J. I., 1981. In: *Physical Processes in Red Giants,* p. 285, eds Iben, I. Jr & Renzini, A., Reidel, Dordrecht, Holland.
Cohen, J., 1976. *Astrophys. J.*, **203,** L127.
Cram, L. E., 1972. *Sol. Phys.*, **22,** 375.
Cram, L. E. & Mullan, D. J., 1985. *Astrophys. J.*, **294,** 626.
Deutsch, A. J., 1960. In: *Stellar Atmospheres, Stars and Stellar Systems,* Vol. VI, ed. Greenstein, J. L.
Dupree, A. K., 1976. In: *Physique des Mouvements dans les Atmospheres Stellaires*, p. 439, eds Cayrel, R. & Steinberg, M., CNRS, Paris.
Dupree, A. K., Hartmann, L. & Avrett, E. H., 1984. *Astrophys. J.*, **281,** L37.
Dupree, A. K., Avrett, E. H., Hartmann, L. & Smith, G., 1984. In: *Proc. 4th European IUE Conference,* Rome, Italy, p. 191, RSA SP-218.
Goldberg, L., 1979. *Q. Jl. R. astr. Soc.*, **20,** 361.
Goldberg, L. *et al.*, 1982. In: *Second Cambridge Workshop on Cool Stars, Stellar Systems and the Sun,* p. 131, eds Giampapa, M. S. & Golub, L., SAO Special Report 392.
Grant, I. P. & Peraiah, A., 1972. *Mon. Not. R. astr. Soc.*, **160,** 239.
Hartmann, L., 1983. In: *Highlights of Astronomy,* p. 549, Vol. 6, ed. West, R. M.
Hartmann, L. & MacGregor, K. B., 1980. *Astrophys. J.*, **242,** 260.
Hartmann, L., Dupree, A. K. & Raymond, J. C., 1981. *Astrophys. J.*, **246,** 193.
Hummer, D. S. & Rybicki, G., 1968. *Astrophys. J.*, **153,** L107.
Jefferies, J. & Thomas, R., 1959. *Astrophys. J.*, **129,** 401.
Kuhi, L. V., 1974. In: *Highlights of Astronomy,* p. 121, Vol. 3, ed. Contopoulos, G., Reidel, Dordrecht, Holland.
Kunasz, P. B. & Hummer, D. G., 1974. *Mon. Not. R. astr. Soc.*, **166,** 57.
Linsky, J. L., 1980. *Ann. Rev. Astr. Astrophys.*, **18,** 439.
Mallia, E. A. & Pagel, B. E. J., 1978. *Mon. Not. R. astr. Soc.*, **184,** 55.
Mallik, S. V., 1982. *J. Astrophys. Astr.*, **3,** 39.
Mihalas, D., 1978. *Stellar Atmospheres,* 2nd edn, Freeman, San Francisco.
Mihalas, D., 1979. *Mon. Not. R. astr. Soc.*, **189,** 671.

Mihalas, D., Kunasz, P. B. & Hummer, D. G., 1975. *Astrophys. J.,* **202,** 465.
Newell, R. T. & Hjellming, R. M., 1982. *Astrophys. J.,* **263,** L85.
Peraiah, A., 1980a. *Acta. astr.,* **30,** 525.
Peraiah, A., 1980b. *J. Astrophys. Astr.,* **1,** 101.
Peraiah, A., 1981. *Astrophys. Space Sci.,* **77,** 243.
Peraiah, A. & Grant, I. P., 1973. *J. Inst. Maths Applcs,* **12,** 75.
Reimers, D., 1975. In: *Problems in Stellar Atmospheres and Envelopes,* eds Baschek, B., Kegel, W. H. & Traving, G., Springer-Verlag, New York.
Reimers, D., 1977. *Astr. Astrophys.,* **57,** 395.
Reimers, D., 1981. In: *Physical Processes in Red Giants,* p. 269, eds Iben, I. Jr & Renzini, A., Reidel, Dordrecht, Holland.
Stencel, R. E., 1978. *Astrophys. J.,* **223,** L37.
Stencel, R. E. & Mullan, D. J., 1980. *Astrophys. J.,* **238,** 221.
Stencel, R. E., Mullan, D. J., Linsky, J. L. & Worden, S. P., 1980. *Astrophys. J. Suppl.,* **44,** 383.
Stencel, R. E., Linsky, J. L., Brown, A., Jordan, C., Carpenter, K. G., Wing, R. F. & Czyzak, S., 1981. *Mon. Not. R. astr. Soc.,* **196,** 47P.
Trimble, V., 1984. *Comm. Astrophys.,* **10,** 167.
Weymann, R., 1962. *Astrophys. J.,* **136,** 844.
White, N. M., Kreidl, T. J. & Goldberg, L., 1982. *Astrophys. J.,* **254,** 670.
Wilson, O. C., 1960. *Astrophys. J.,* **131,** 75.
Wischnewski, E. & Wendker, H. J., 1981. *Astr. Astrophys.,* **96,** 102.